INSTITUTE FOR NUCLEAR STUDY
UNIVERSITY OF TOKYO
Tanashi, Tokyo 188
Japan

INS-TH-159
April 10, 1984

Test of the Delay Line for Z-readout of the TOPAZ Inner Drift Chamber

K. Shiino, A. Imanishi, T. Ishii, S. Kato, K. Kono, H. Masuda, T. Morimoto, K. Norimura, T. Ohshima, H. Okuno, K. Ukai and M. Yoshioka

INS-TH-159
April 10, 1984

Test of the Delay Line for Z-readout of the TOPAZ Inner Drift Chamber

K. Shiino, A. Imanishi, T. Ishii, S. Kato, K. Kono, H. Masuda, T. Morimoto, K. Norimura, T. Ohshima, H. Okuno and K. Ukai

Institute for Nuclear Study, University of Tokyo

(April 10, 1984)

We have tested the zig-zag delay lines for z-readout of the TOPAZ inner drift chamber. Using the delay line of 69 cm long and 10 cm wide having the characteristic delay of 5.9 ns/cm, spatial resolution of 8.5 mm in FWHM is obtained for the minimum-ionizing particles with the gas mixture of 50% argon and 50% ethane.

1. Introduction

In the TOPAZ inner drift chamber, information on the z-coordinate is used mainly for triggering purposes in order to reject the background from the beam-gas and beam-wall interactions and cosmic rays. For these in mind, we have examined the possibility to use the delay line scheme for the z-readout. Figure 1 shows the schematic drawing of the inner drift chamber. The cylindrical chamber is divided into 32 sectors for the z-readout. In each sector, eight layers of delay lines are placed as cathodes of the drift chamber. As the number of the signal wires is 64 for the innermost layer and 128 for the other layers, one delay line covers two and four anode wires, respectively. The reason for these segmentations of the delay line readout is discussed elsewhere[1]. With this configuration, the total number of delay lines is 256. Compared to the cathode strip readout previously proposed[2], the number of readout channels is largely reduced and the structure of the end-plate is simplified.

A schematic diagram of the z-track finding is shown in Fig.2. The induced signal on the delay line travels in two opposite directions toward the ends. A measurement of time difference between two signals at both ends gives us the particle position along the anode wire. Information of this time difference is recorded on shift registers. Shift registers are started by the signal arriving earlier among the two signals from both ends and are stopped by the other. The position information is stored in the shift registers as a bit pattern. When the characteristic delay of the delay line and the clock frequency of the

shift registers are properly chosen in such a way that the Δz/bit is proportional to the radius r of the delay line location, the hit bits for the particle track originating from the beam crossing area can be nicely aligned in the same column. This characteristic bit pattern in the shift registers can be quickly checked and whether the track originates from the beam crossing area or not is determined. Further details will be reported shortly after

As an interval of the beam crossing at TRISTAN is 2.5 μs, the decision to trigger the data aquisition system should be done within 1 - 2 μs. When we take into account the drift time of about 200 ns, the cable delay of about 150 ns and the delay in the trigger logic of about 350 ns, the available time interval for the maximum delay on the delay line is about 650 ns. Therefore the characteristic delay of the delay line should be 3 - 4 ns/cm.

2. Zig-zag Delay Line

Various delay lines with different structures were already developed by many groups for each special purpose. Among them the shifted zig-zag delay lines [3)-6)] are best suited for the present application, because (1) the thickness of the delay line can be very small (100-150μm thick and 10^{-3} X_0) and (2) the delay line can be used as a cathode of the drift chamber.

A basic structure of the delay line is shown in Fig.3. Shifted zig-zag patterns made of copper strips sandwich the Kapton film of 50-150 μm thick. Characteristics of the delay

line can be calculated approximately by using the following equations[3];

$$L_p \simeq 3a \left(3 + 5\sqrt{\frac{s}{w}} \right) \quad \text{nH} , \tag{1}$$

$$C_p \simeq \frac{\varepsilon}{5} \left(1 + \frac{w}{e} \right) a \quad \text{pF} , \tag{2}$$

$$Z_o = \sqrt{L_p / C_p} \quad \Omega , \tag{3}$$

$$\tau_d \simeq \sqrt{L_p C_p} / 2(s + w) \quad \text{ns/ m} , \tag{4}$$

$$R = Ro\ lo / e'\ w \quad \Omega , \tag{5}$$

where L_p and C_p denote the inductance and the capacitance per unit period of the zig-zag. Z_o, R, and τ_d denote the characteristic impedance, the total resistance and the characteristic delay of the delay line, respectively. W, S, a, e and e' denote the geometrical parameters shown in Fig.3, where a is given in cm. ε is the relative dielectric constant of the insulating material. R_o and l_o denote the volume resistivity and the total length of the strip line. Comparisons between the calculation and the measured value are shown in Table 1 for the typical delay line. The agreements between the calculation and the measurement is relatively good for the line impedance and the characteristic delay. However the total resistance R differs about 50%. This may be due to the incorrect estimation of the Cu-strip thickness. In the etching process of the Cu-strip, the thickness may be reduced.

In the inner drift chamber, eight cylindrical layers of

delay lines are placed at different radii, but the azimuthal segmentations are the same. Although the zig-zag pattern on each layer has different dimensions, these lines can be fabricated from the same pattern masks by changing only the magnification factor, if the characteristics of each line fall in a resonable range. When we define the magnification factor to be unity for the reference layer at r = 25.6 cm, characteristics of the delay lines are calculated as shown in Fig.4. Points in the figure show the values expected for the delay lines at the designed radii. The characteristic delays are in the range from 2.7 ns/cm to 3.8 ns/cm which is accepted from the viewpoint of the triggering mentioned before.

Transmission characteristics of the delay line whose characteristics are shown in Table 1 were measured for the square pulse of 2V high and 100 ns wide. Fig.5 shows the transmitted wave form for different line lengths. Fig.6 shows the summary of the rise time and the pulse height attenuation as a function of the delay line length. The pulse height decreases to 65% when the square pulse traveled on the delay line of 160cm long. The rise time (0 - 50%), t_{50}, defined by $A(t_{50}) = 0.5X\ A_{max}$ is about 27ns for the 160cm delay line.

Signal transmissions were measured as a function of the signal frequency. Results are shown in Fig.7. For the delay line of 69cm long, 50% transmission was obtained for the frequency up to 20 MHz.

3. Test Chamber

To study the performance of the delay line, we assembled a

test chamber as shown in Fig.8. The square box of 201mm wide x 730 long x 126 high contains the 40 sensing anode wires and 8 layers of delay line cathodes. Wire configurations are the same designed for the inner drift chamber. The gold-plated tungusten wires of 30 μm in diameter were used as anode wires and the copper-berrylium wires of 100μm in diameter were used as potential wires. All wire spacings are 6mm. Three types of delay lines with different widths are tested. In this report, the results on the delay line listed in Table 1 is mainly described, because its width covers the whole anode wires across the beam.

4. Readout Electronics

Each end of the delay line was coupled to the preamplifier via a bifilar transformer shown in Fig.9 as studied by R. Bosshard et al.[3] This transformer works to 1) step up the signal volage by a factor of 2, 2) to increase the impedance by a factor of 4 and 3) to convert the balanced signal to the unbalanced signal. The circuit diagram of the preamplifier is shown in Fig.10, which was originally developed by V. Radeka.[6] The signal shaping was done by use of the pole-zero filter with the time constant of 150 ns.

Output signals from the preamplifier were sent to the AC-coupled amplifiers and leading-edge discriminators as shown in the electronics block diagram of Fig.11. Time difference between signals from both ends of the delay line was measured by use of the LeCroy qvt or the LeCroy TDC 2228.

5. Results

The delay line performance was measured in the drift chamber operated with the gas mixtures of $Ar(90\%)/CH_4(10\%)$ and $Ar(50\%)/C_2H_6(50\%)$. The test was made by use of the ^{55}Fe X-rays and the 0.5 GeV/c electron beam from the electron synchrotron.

Fig.12 shows the pulse shape from the preamplifier for the ^{55}Fe source placed at the center of the delay line. As a reference, the anode signal is also shown in the lowest line. The rise time (t_{50}) of the delay line signal is about 15 ns. Although the impedance of the preamplifier was carefully adjusted, the small preceeding signals were observed. The threshold of the leading-edge discriminater was set above this noise level and the position resolutions were measured with the well-collimated (3mm in FWHM) X-ray source. A typical example of the position spectrum is shown in Fig.13 for the gas mixture of $Ar(90\%)/CH_4(10\%)$ at H.V.= 1.9kV. A FWHM resolution of about 6mm was obtained over the H.V. range between 1.75 kV and 1.90 kV. The relative resolution $\Delta L/L$ is estimated to be 0.8% in FWHM. In this H.V. range, the collected charge on the anode wire starts to saturate.

The delay line was also tested with the momentum-analyzed electron beam. The beam was collimated with the use of the 3mm-thick scintillation counter. For the minimum ionizing particles, the energy loss in the drift chamber is about 1/3 of the ^{55}Fe X-ray energy. Therefore the threshold level of the discriminater had to be carefully adjusted. The gas mixture used in this measurement was $Ar(50\%)/C_2H_6(50\%)$. Fig.14 shows the detection efficiency versus the applied voltage on the anode. For the

anode signal, the efficiency plateau is reached at H.V. = 2.3kV. The efficiency for the delay line readout was defined in such a way that both signals exceeded the threshold level of the discriminater and the time difference fell in the predetermined region. The efficiency plateau is reached at H.V. = 2.55kV. This H.V. difference corresponds to the avalanche size difference of a factor 2. It is essentially important to reduce this discrepancy for the low voltage operation of the drift chamber. This can be realized only by reducing the noise contribution to the delay line readout electronics.

The results on the position measurement are shown in Fig.15 and Fig.16, where the data was taken at H.V. = 2.55kV. The position linearity is good over the delay line length of 60cm and the position resolution is around 8.5 mm in FWHM.

We also tested the delay line performance for the inclined tracks. For the beam injection angle of 45° to the normal of the delay line plane, the position resolution was not deteriorated, although the pulse height increased in proportion to the track length in the drift chamber.

6. Summary and Discussion

Comparisons of the delay line performance are shown in Table 2. Our results are comparable to the others. The obtained resolution is accurate enough to be used in the inner drift chamber for the triggering purpose. To improve the position resolution and the detection efficiency, further reduction of the electronics noise is essential. The coupling between the delay

line and the preampliffier is the key factor to achieve the good performance at the lower anode voltage. We are making further efforts to increase the signal pick-up efficiency of the delay line and to reduce the noise of the preamplifier.

References

1. T. Ohshima, Principle of the Z-track Finder, Oct.20, 1983.
2. TOPAZ Proposal TRISTAN-Exp-002, Jan. 1983.
3. R. Bosshard et al, IEEE Vol NS-22, 2053 (1975).
4. M. Atac et al, IEEE Trans. on Nucl. Sci. NS-24 195(1977).
5. A. L. Sessoms et al, IEEE Trans. on Nucl. Sci. NS-25 38(1978).
6. V. Radeka, IEEE Trans. on Nucl. Sci. NS-21, 51(1974).

Figure Captions

Fig. 1 Schematic drawing of the inner drift chamber.

Fig. 2 Principle of the Z-track finding in the inner drift chamber.

Fig. 3 Basic structure of the shifted zig-zag delay line.

Fig. 4 Characteristics of the delay line as a function of the magnification factor. The delay line at r = 25.6cm is chosen as a reference whose magnification factor is unity.

Fig. 5 Transmission of the square pulse in delay lines of various lengths.

Fig. 6 Rise time and pulse height attenuation as a function of the line length.

Fig. 7 Frequency responce of the delay line.

Fig. 8 Schematic drawing of the test chamber.

Fig. 9 Bifilar transformer.

Fig.10 Preamplifier circuit.

Fig.11 Electronics block diagram.

Fig.12 Pulse shapes for the ^{55}Fe X-ray.

Fig.13 Position spectrum for the ^{55}Fe X-ray.

Fig.14 Detection efficiency vs. H.V.

Fig.15 Position spectra for the 500 MeV/c electron beam.

Fig.16 Position linearity and resolution for the 500 MeV/c electron beam.

Table 1

Geometries

Strip spacing	s =	3.2 mm
Strip width	w =	3.2 mm
Line width	a =	10 cm
Zig-zag period	2 (s+w) =	12.8 mm
Thickness of the spacer	e =	50 μm
Thickness of the Cu-strip	e' =	36 μm
Length	L =	76 cm

Characteristics of the Delay Line

	Calculated Values	Measured Values
Impedance(Z_o)	34.6 Ω	31 Ω
Characteristic Delay(τ_d)	5.4 ns/cm	5.9 ns/cm
Total Resistance(R)	2.8 Ω	4.1 Ω

Table 2. Zig-zag Delay Line Performance

GROUP	Delay Line Length(cm)	Position Resolution F W H M (%)	Tested with
BNL (1975) Bosshard et al	20	1.0	β - ray
FNAL Atac et al.	50	0.5 0.7	^{55}Fe source muon beam
Harvard (1977) Sessons et al.	120	0.83	
OURS (1984) Shiino et al.	69	0.8 1.2	^{55}Fe source electron beam

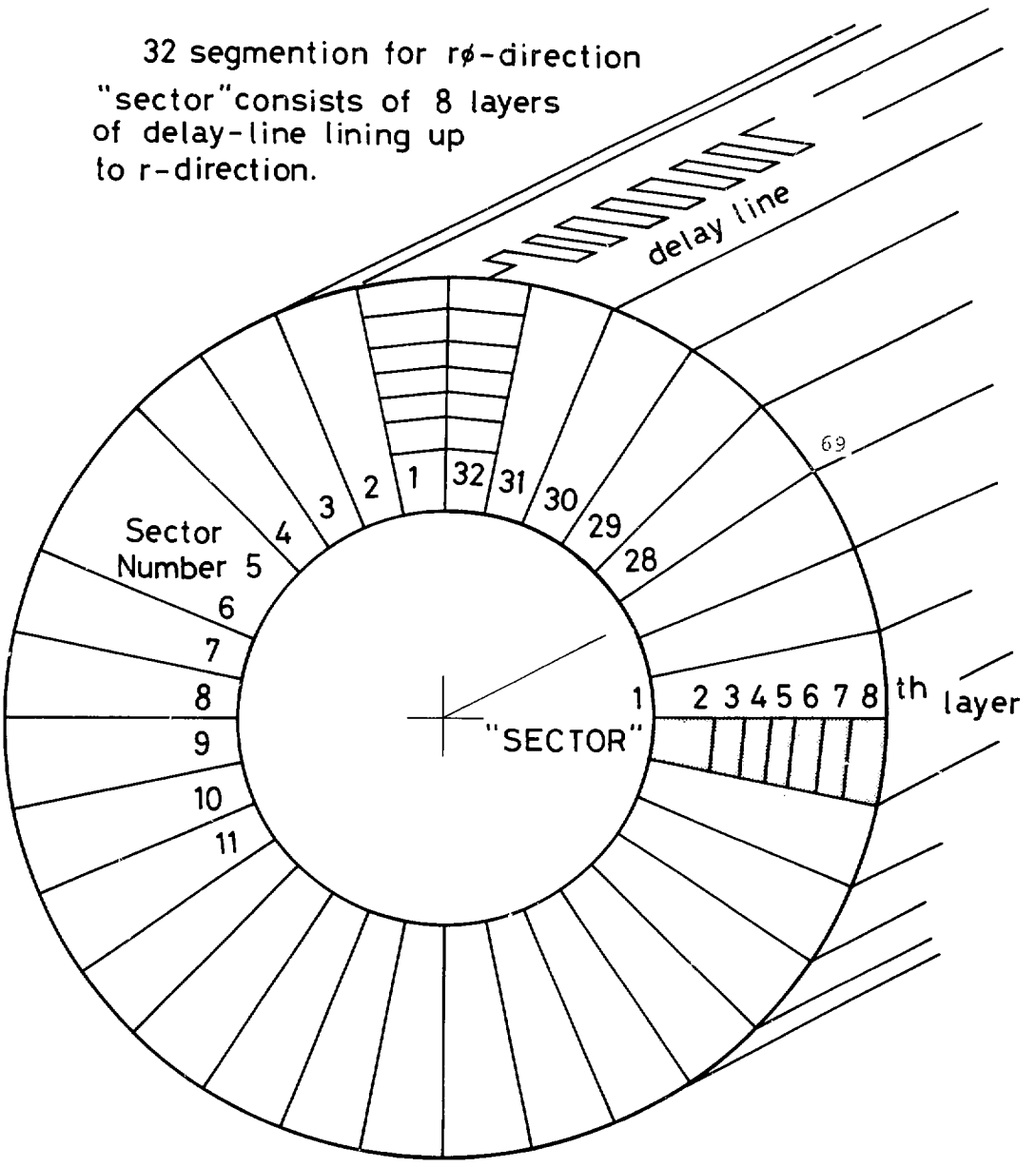

Fig.1 Schematic drawing of the inner drift chamber.

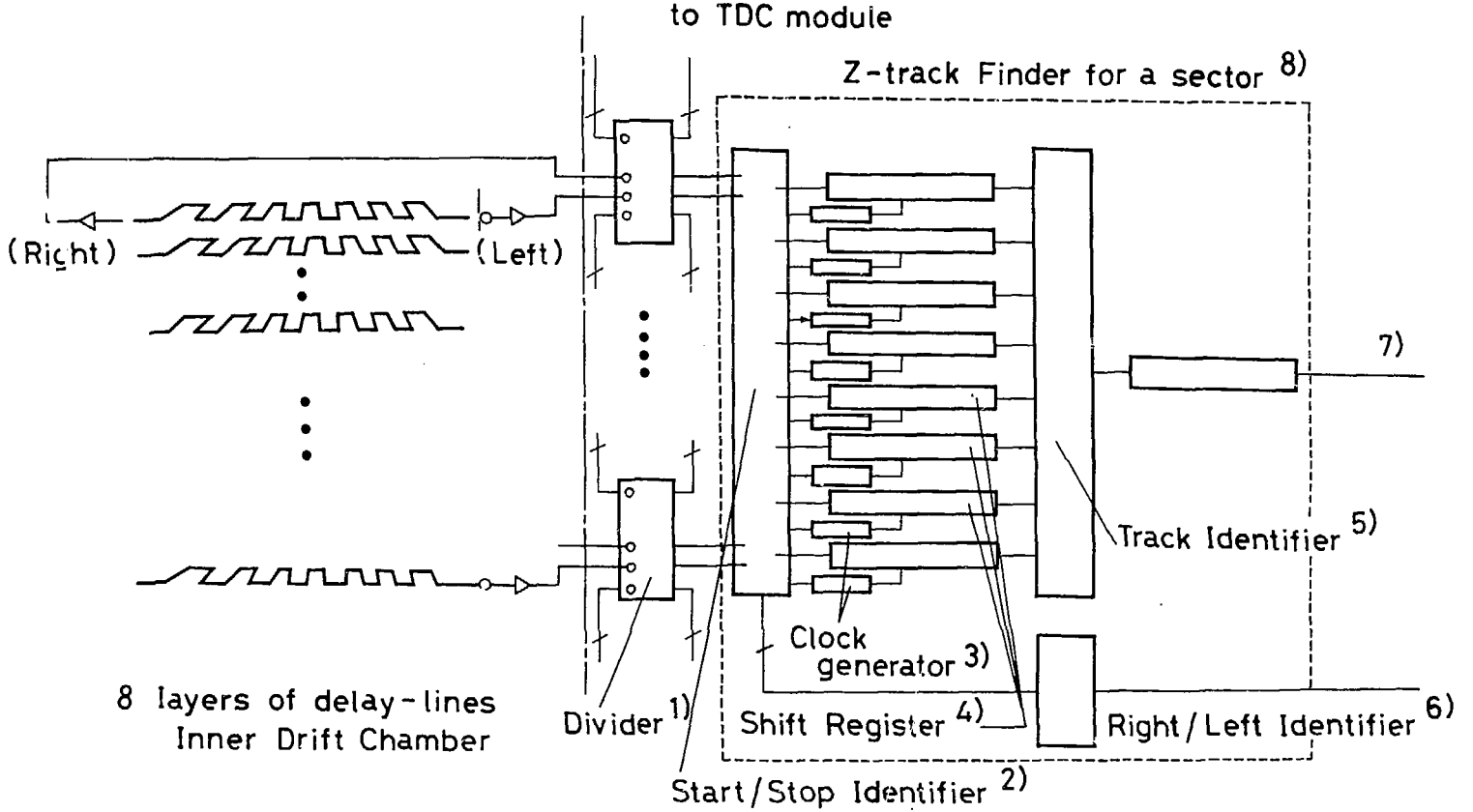

Schematic Diagram for Z-track finding

Fig.2 Principle of the Z-track finding in the inner drift chamber.

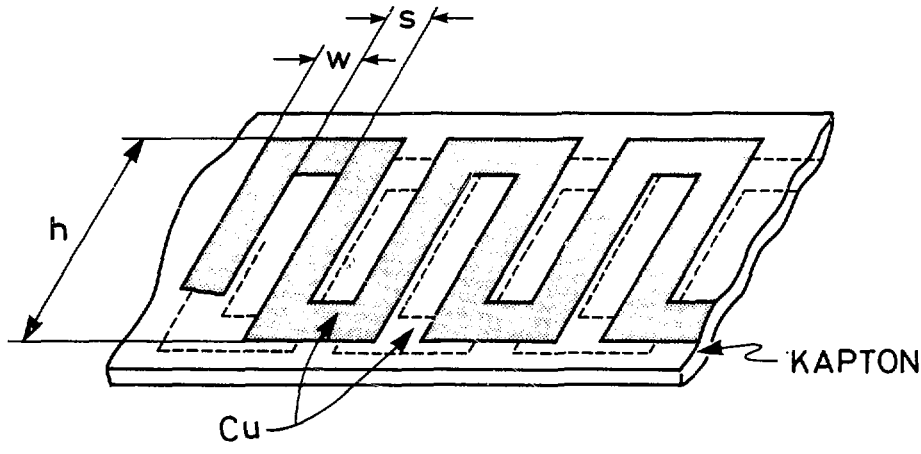

Fig.3 Basic structure of the shifted zig-zag delay line.

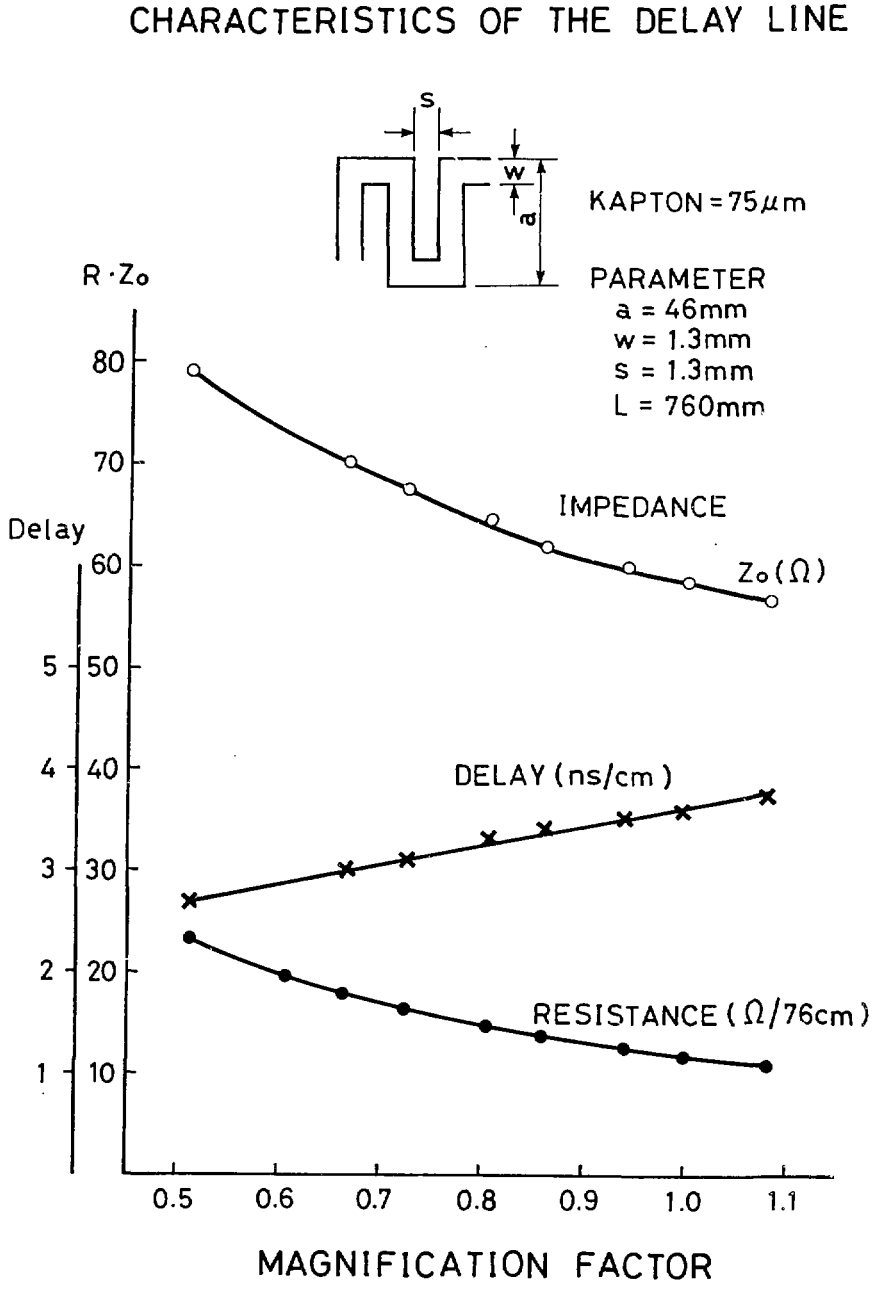

Fig.4 Characteristics of the delay line as a function of the magnification factor. The delay line at r = 25.6 cm is chosen as a reference whose magnification factor is unity.

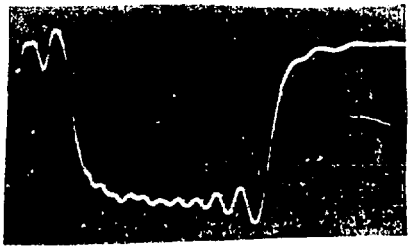

(a) L = 25.6 cm

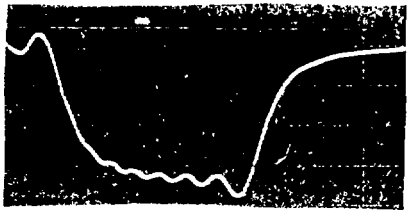

(b) L = 64 cm

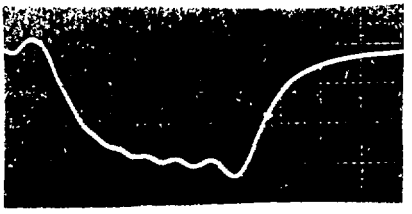

(c) L = 89.6 cm

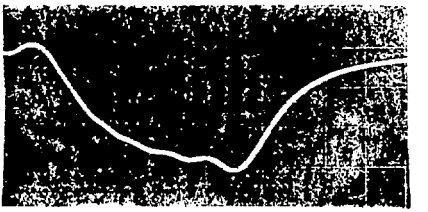

(d) L = 128 cm

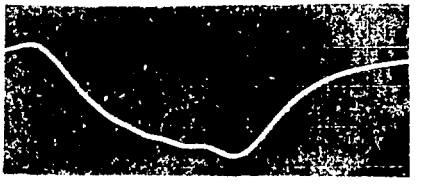

(e) L = 153.6 cm

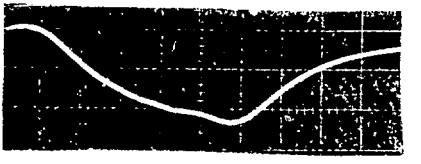

(f) L = 192 cm

Fig.5 Transmission of the square pulse in delay lines of various lengths. Input pulses: 2 V in height and 100 ns in width. Vertical scale: 0.5 V/div. Horizontal scale: 20 ns/div.

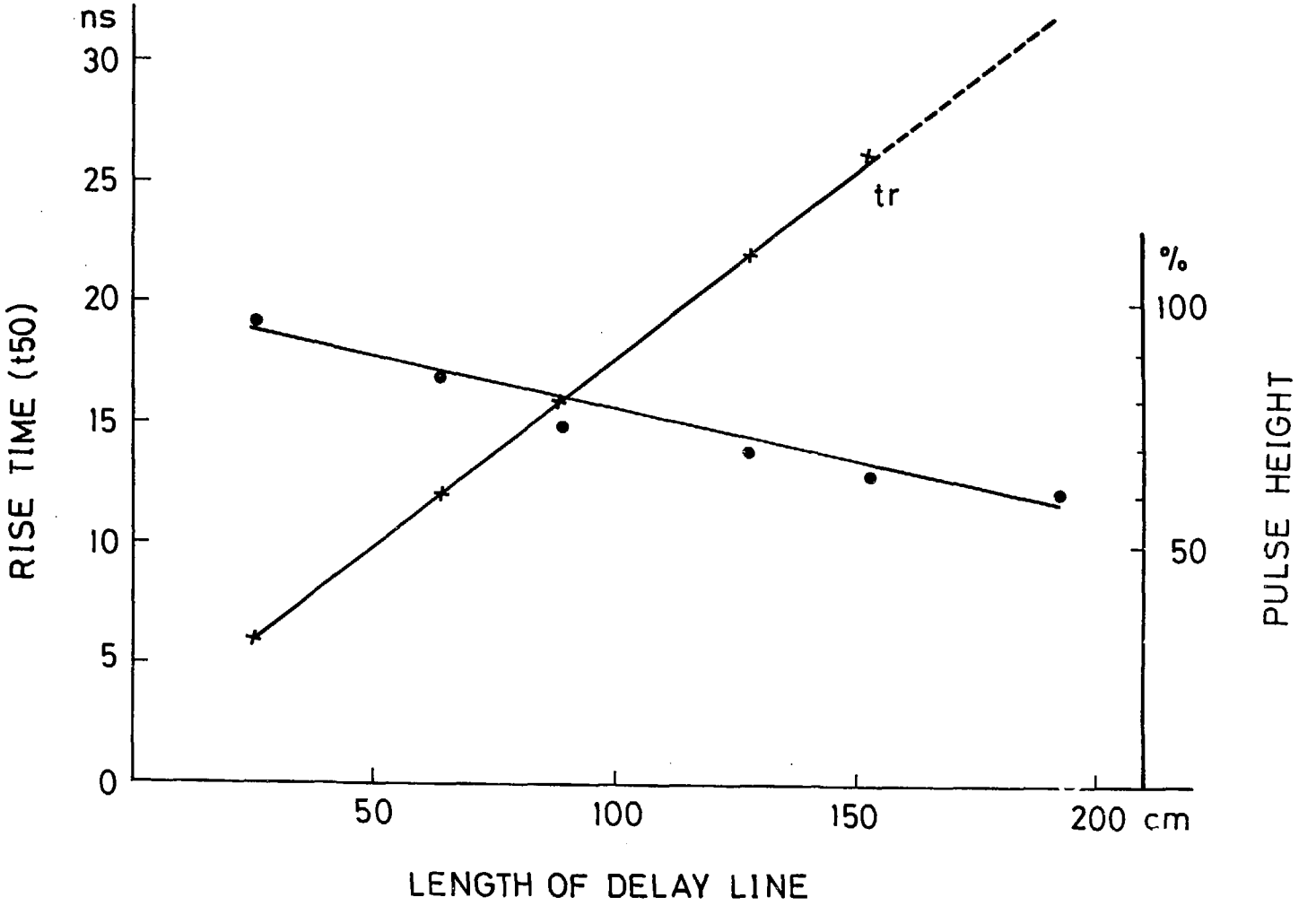

Fig.6 Rise time and pulse height attenuation as a function of line length.

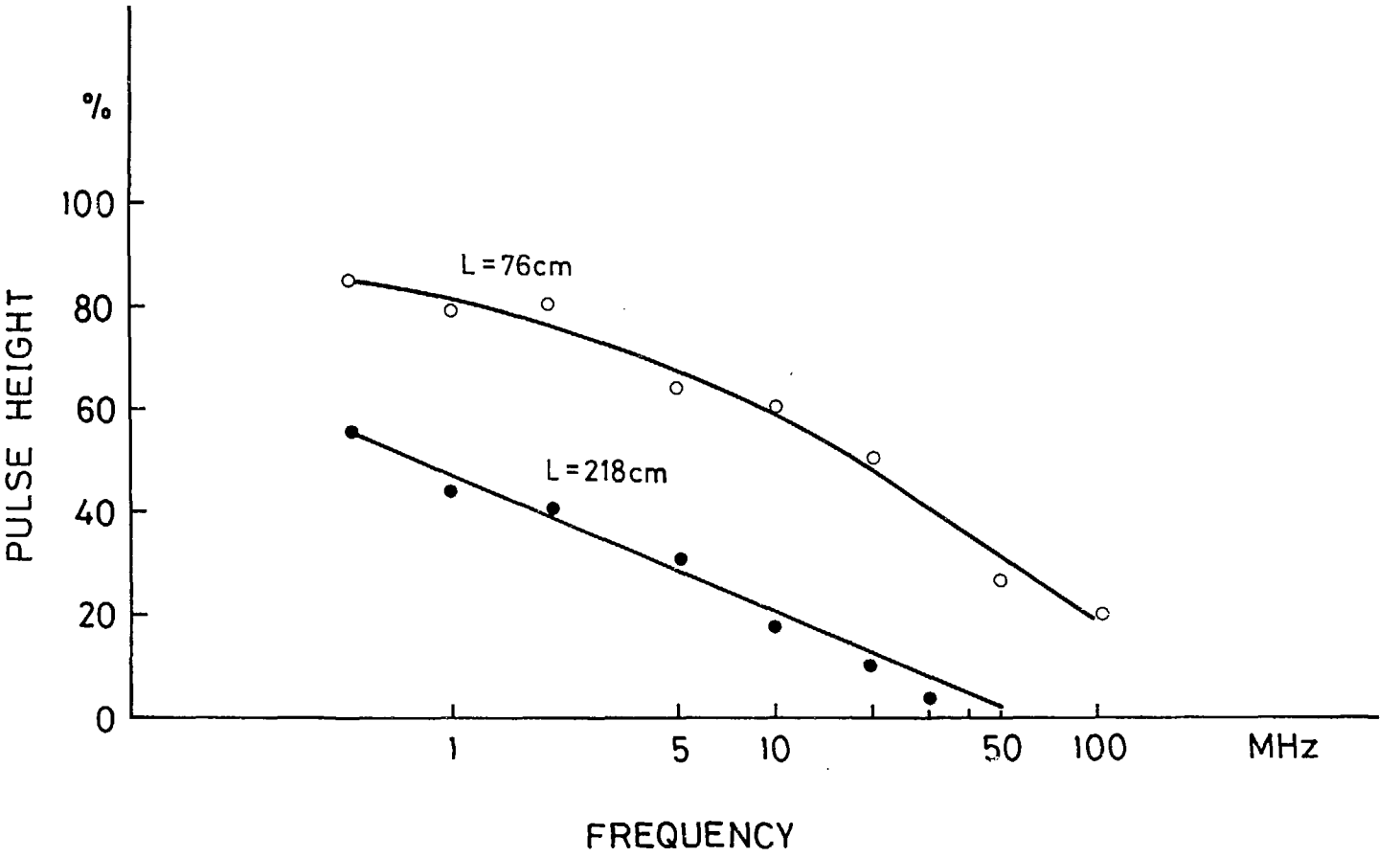

Fig.7 Frequency responce of the delay line.

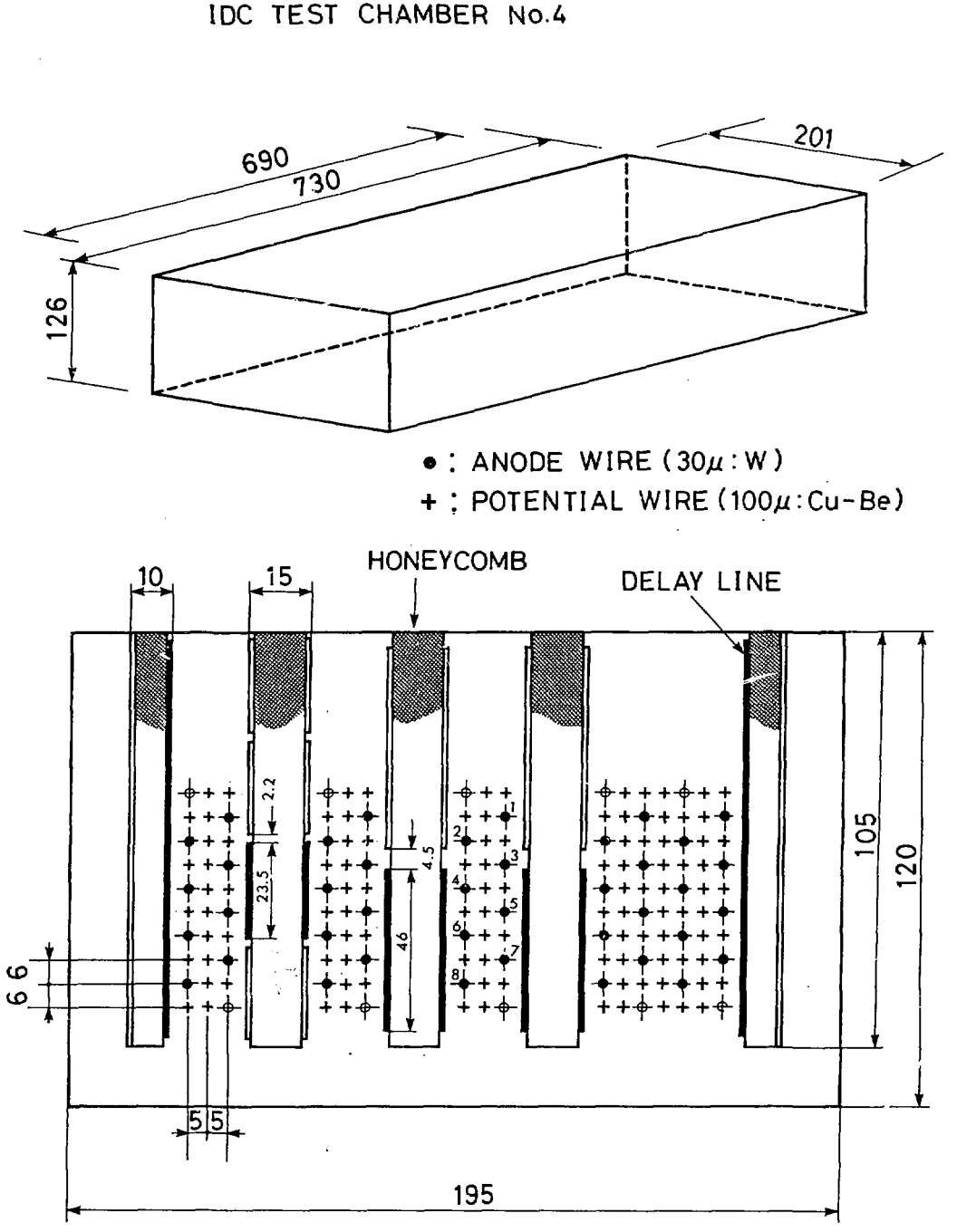

Fig.8 Schematic drawing of the test chamber.

Bifilar Coil

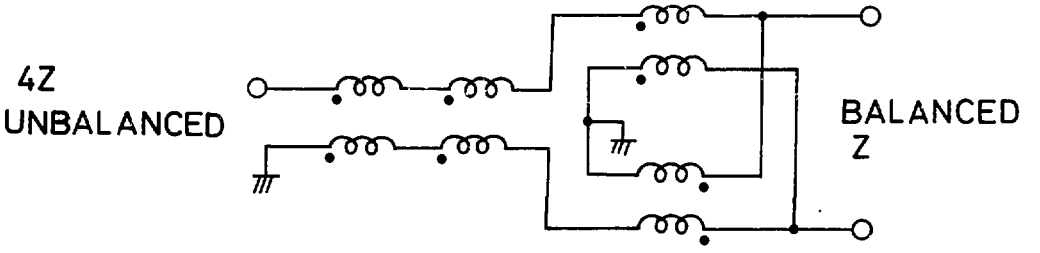

Fig.9 Bifilar transformer.

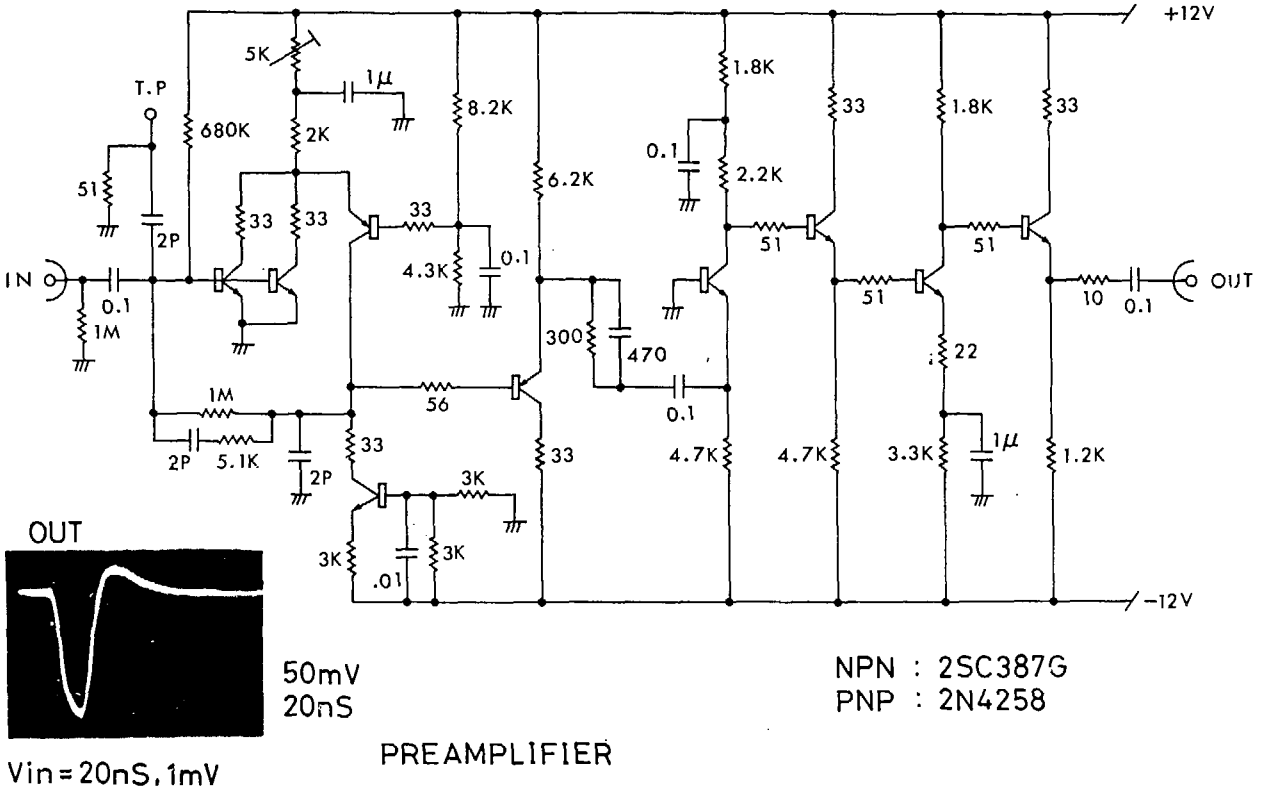

Fig.10 Preamplifier circuit.

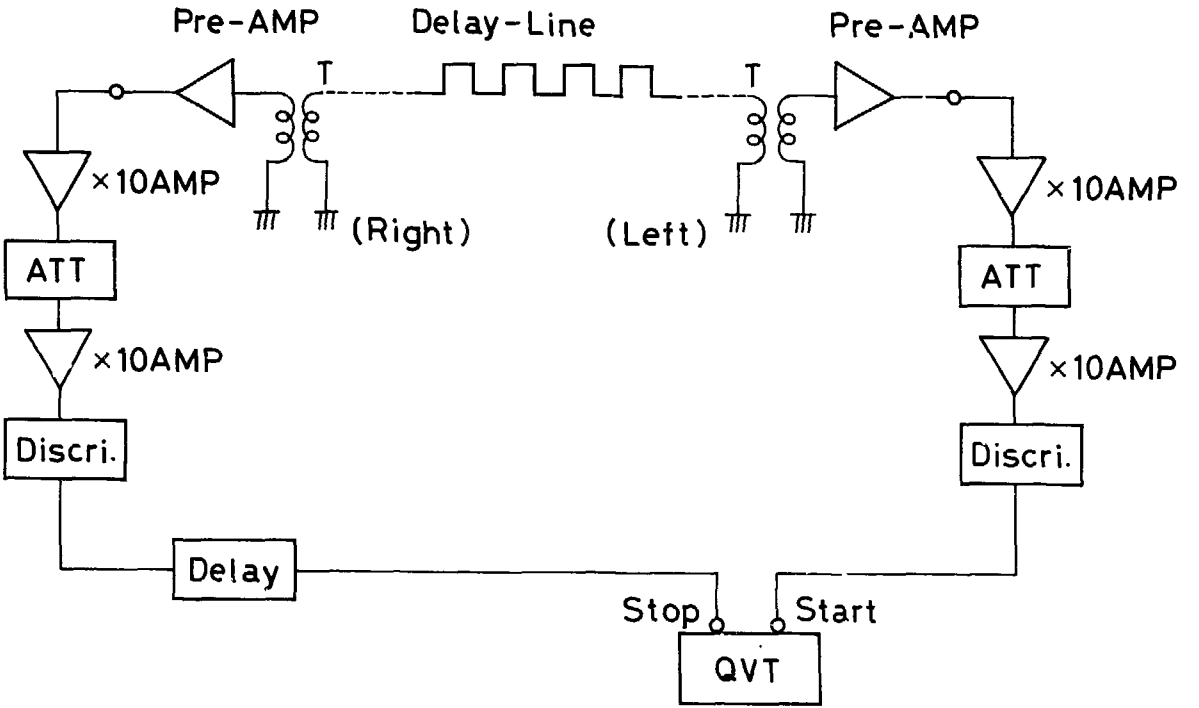

Fig.11 Electronics block diagram.

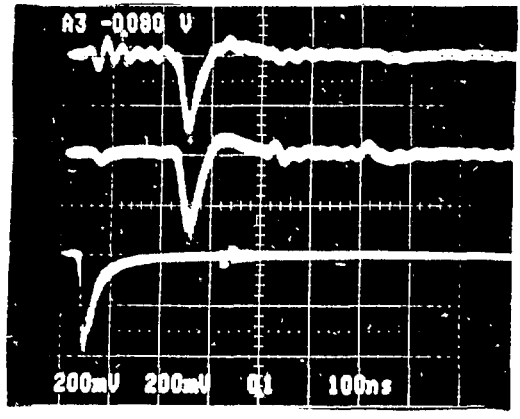

Fig.12 Pulse shapes for the ^{55}Fe X-ray.

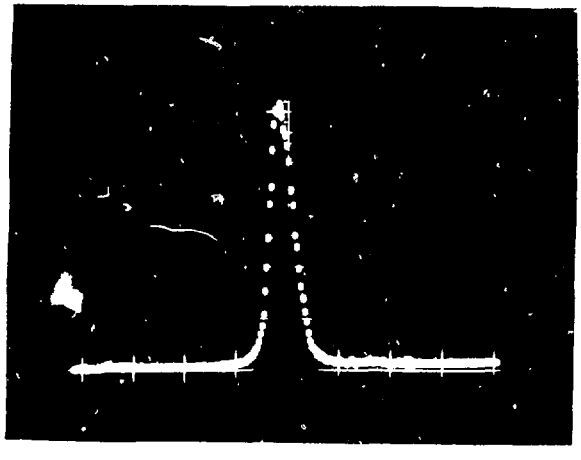

Fig.13 Position spectrum for the ^{55}Fe X-ray.

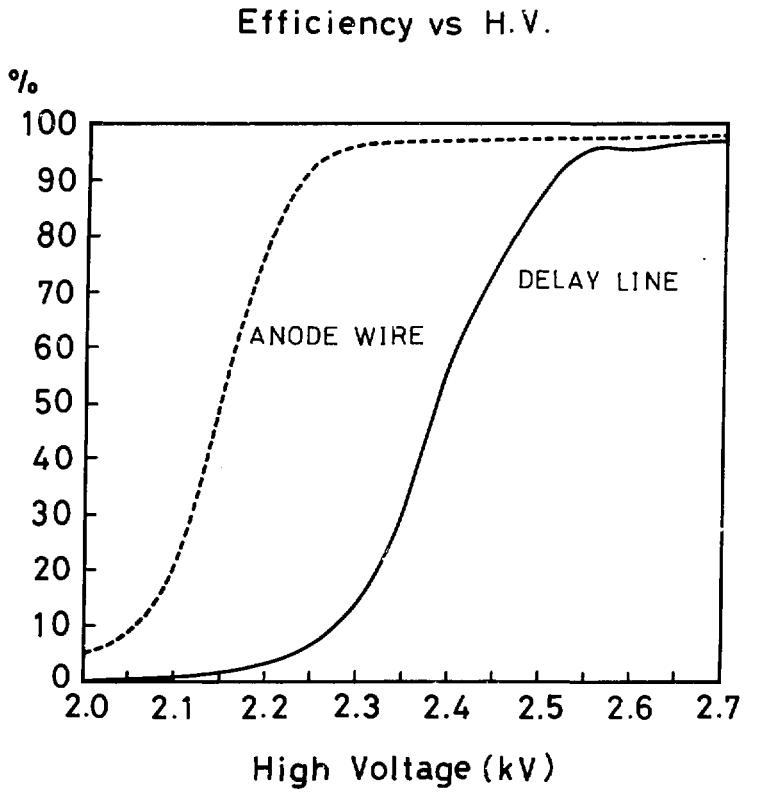

Fig.14 Detection efficiency vs. H.V..

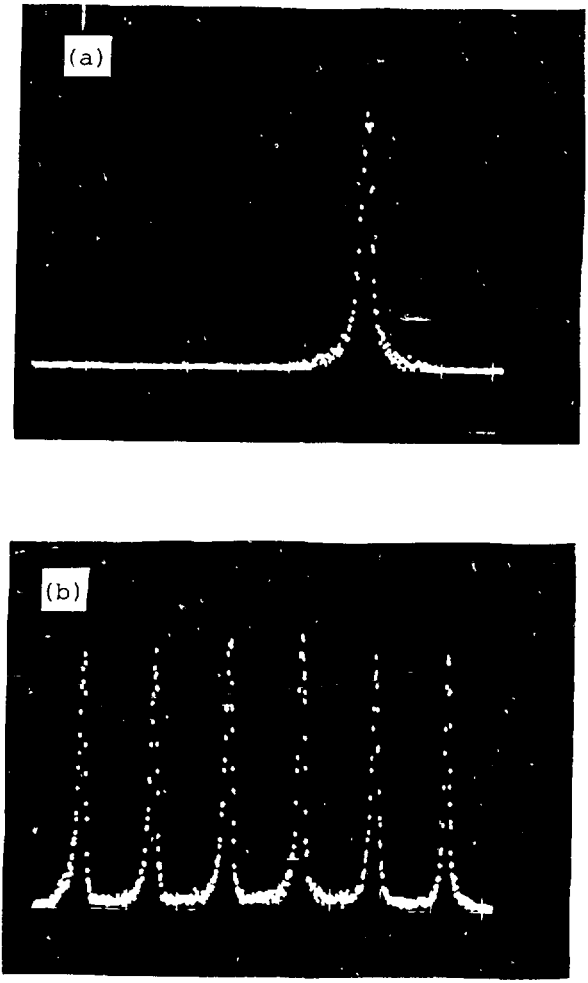

Fig.15 Position spectra for the 500MeV/c electron beam.

(a) Spatial resolution (FWHM) ≃ 0.8 cm.

(b) Position step = 10 cm.

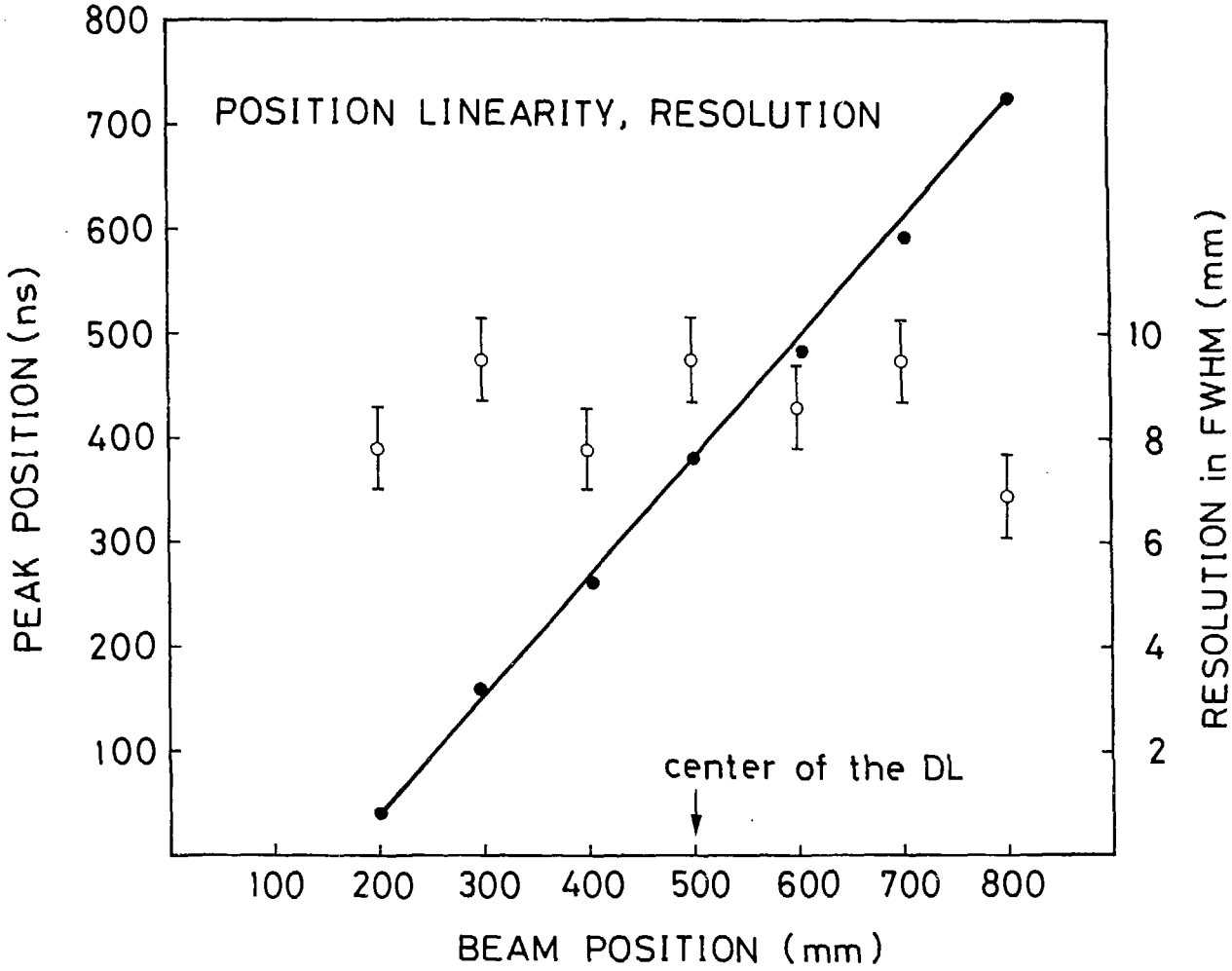

Fig.16 Position linearity and resolution for the 500MeV/c electron beam.